IEEE Access
Multidisciplinary ⋮ Rapid Review ⋮ Open Access Journal

Received November 20, 2021, accepted December 22, 2021, date of publication December 24, 2021,
date of current version January 6, 2022.

Digital Object Identifier 10.1109/ACCESS.2021.3138371

Original Application of Stop-Band Negative Group Delay Microwave Passive Circuit for Two-Step Stair Phase Shifter Designing

BLAISE RAVELO[1], (Member, IEEE), GLAUCO FONTGALLAND[2], (Senior Member, IEEE), HUGERLES S. SILVA[3,4], (Member, IEEE), JAMEL NEBHEN[5], (Member, IEEE), WENCESLAS RAHAJANDRAIBE[6], (Member, IEEE), MATHIEU GUERIN[6], (Member, IEEE), GEORGE CHAN[7], (Senior Member, IEEE), AND FAYU WAN[1], (Member, IEEE)

[1]School of Electronic and Information Engineering, Nanjing University of Information Science & Technology, Nanjing 210044, China
[2]Applied Electromagnetic and Microwave Laboratory, Federal University of Campina Grande, Campina Grande 58429-830, Brazil
[3]Departamento de Eletrónica, Telecomunicações e Informática, Instituto de Telecomunicações, Universidade de Aveiro, Campus Universitário de Santiago, 3810-193 Aveiro, Portugal
[4]University of Brasília, Brasilia 70910-900, Brazil
[5]College of Computer Engineering and Sciences, Prince Sattam Bin Abdulaziz University, Al-Kharj 11942, Saudi Arabia
[6]Aix-Marseille University, CNRS, University of Toulon, IM2NP UMR7334, 13397 Marseille, France
[7]ASM Pacific Technology Ltd., Hong Kong

Corresponding author: Jamel Nebhen (j.nebhen@psau.edu.sa)

This work was supported in part by the National Natural Science Foundation of China (NSFC) under Grant 61971230, in part by the Jiangsu Specially Appointed Professor Program and Six Major Talents Summit of Jiangsu Province under Grant 2019-DZXX-022, in part by the Startup Foundation for Introducing Talent of the Nanjing University of Information Science and Technology (NUIST), in part by FCT/MCTES through national funds and, when applicable, co-funded by EU funds under Project UIDB/50008/2020 and Project UIDP/50008/2020, and in part by the Deanship of Scientific Research at Prince Sattam Bin Abdulaziz University, Saudi Arabia.

ABSTRACT This paper investigates on the theorization, design, fabrication and measurement of original phase shifter (PS) operating with two-step stair phase behavior. The innovative stair PS is designed with unfamiliar stop-band (SB) negative group delay (NGD) passive circuit. The elementary unfamiliar SB-NGD topology constituted by resistive, inductive, and capacitive lumped network is described. Acting as an RF and microwave circuit, the S-matrix model is expressed in function the RLC-network parameters. Thus, the canonical form of unfamiliar SB-NGD transfer function (TF) represented by the transmission coefficient is established. The unfamiliar SB-NGD circuit equations in terms of the NGD parameters are formulated. The established theory is validated comparing the calculated, simulated, and measured S-parameters and group delays (GDs). Results with a very good agreement showing unfamiliar SB-NGD behavior are observed around the central frequency 2.45 GHz and bandwidth of 100 MHz. An innovative application of unfamiliar SB-NGD function for the communication system front-end is developed. The developed application concept of unfamiliar SB-NGD circuit is illustrated by designing a microwave device operating as a PS presenting a two-step stair response completely original behavior. The basic theory, design and implementation of the two-step stair PS concept are introduced. To validate the two-step stair PS principle, a proof of concept (PoC) is designed based distributed element based inductive and capacitive microstrip elements. The simulated and measured results of the PS PoC are in good agreement. The experimental results confirm the feasibility of two-step stair PS with phase jumping from $-70°\pm4°$ (from 2 GHz to 2.3 GHz) to $-104°\pm2°$ (from 2.6 GHz to 3.0 GHz). The investigated unfamiliar SB-NGD function-based stair PS is promising for future development 5G and 6G communication system.

INDEX TERMS Circuit theory, innovative concept, design method, microwave circuit, passive topology, S-parameter model, stop-band (SB) negative group delay (NGD), SB-NGD application, stair phase shifter (PS).

I. INTRODUCTION

The massive deployment of 5G technology constitutes a bridging step of future wireless communication. To meet the expected users demand, innovative design of front-end RF and microwave circuit ensuring accurate performance of radiation pattern is necessary [1]. This radiation performance is essentially ensured with improvement of beam-steering antenna array design [2]–[4]. Different antenna array topologies as adaptive [2] and coupled phased looped

The associate editor coordinating the review of this manuscript and approving it for publication was Venkata Rajesh Pamula.

array [3] have been proposed. But these topologies need to be improved to suppress the RF impairment in massive antenna arrays [4]. To increase the compactness and linearity, an innovative topology of metamaterial-based array antenna was proposed [5], [6]. Such antenna arrays operate with linear metamaterial-based phase shifters [7].

The elaboration of negative refractive index (NRI) aspect of metamaterial was an inspiration for the emerging RF and microwave function operating with bandpass (BP) negative group delay (NGD) [8], [9]. The NRI structures are also known to operate with negative group velocity (NGV) effect. The metamaterial BP-NGD circuits were implemented with significantly lossy periodical cells [8], [9]. Therefore, RF and microwave engineers wondered curiously on the existence of BP-NGD circuit application. To answer, tentative applications were suggested [10]–[24]. The BP-NGD function was introduced for adaptative aspect in a microwave signal processing building block [10]. Then, the NGD circuit was also proposed for the compensation of microwave devices [11].

However, the natural NGD application is the group delay (GD) equalization [12]–[14], which was proposed for the microwave signal RC-network based interconnects [12], [13] and also the BP filter GD rabbit ear reduction [14]. So far, the most developed application of unfamiliar BP-NGD function concerns the design of RF and microwave phase shifters (PSs) [15]–[24]. The NGD PS was, recently, exploited to develop innovative topologies of antenna array operating with squint-free beamforming [15]–[21]. This type of NGD antenna array application is fundamentally implemented with non-Foster elements using BP-NGD networks [17], [20], [21]. Another type of innovative application was the design of broadband PS using BP-NGD function operating independently to the frequency [22]–[24].

Further innovative work inspired from this BP-NGD PS will be developed in the present paper. But before this point, it would be interesting to investigate more on the unfamiliar NGD function. Recent investigations from research teams [25]–[32] confirm the diversity of BP-NGD topologies. The BP-NGD effect was verified with absorptive filter [25] and interference techniques [26]. A topology of BP-NGD active circuit was implemented by using microwave transversal filter approach [27]. The complexity leads some research works on the design of compact microwave passive circuits [28], [29]. More extensive microwave function aspect as the dual-band BP-NGD behavior was developed in [30]–[33]. The dual-band NGD functions were also implemented with compact circuits [31], [32] and with multi-coupled lines [33].

Despite the progressive state of the art on the BP-NGD circuit design, due to its unfamiliarity, curious questions are still raised by RF and microwave design engineers about the interpretation of the NGD effect. For a deep illustration, an analogy between the filter theory and the NGD function theory was addressed in [34]. Unlike the filter, the NGD function focuses mainly on the negative sign associated to the GD response and not to the magnitude response [34]–[36]. Different types of NGD function are initiated and identified [35]–[40]. The concept of low-pass (LP) NGD function was proposed in [35]. The BP-NGD [8]–[14], [20]–[29], high-pass (HP) NGD [36]–[38] and stop-band (SB) NGD [39], [40] RF passive circuits transformed from low-pass (LP) NGD cell are introduced.

TABLE 1. State-of-the-art on the different types of NGD circuits.

References	Type	Passive/Active
[13, 34]	LP-NGD	Active circuit
[35-36]	LP-NGD	Passive circuit
[8-9,14, 20,25-26,28-29]	BP-NGD	Passive circuit
[10-11,13,21,27]	BP-NGD	Active circuit
[36-38]	HP-NGD	Passive circuit
[30-33]	Dual-band BP-NGD	Passive circuit
[39-40]	SB-NGD	Passive circuit

Table 1 addresses an overview on the state-of-the-art about the existing different types of NGD function which can be implemented either with passive or active circuits. It is important to note the dual-band NGD circuits as proposed in [30]–[33] are completely and ideally different to the type of SB-NGD circuits.

So far most of available research work on the design of NGD circuits can be described as follows:

- The simplest topologies are designed as LP-NGD type function [13], [34]–[36]. For this type, the group delay (GD) is negative from DC to certain higher frequencies.
- The BP-NGD type function containing lower and upper NGD cut-off frequencies are mainly designed for RF and microwave circuits [15]–[34].
- By means of LP- to HP-NGD circuit transform, circuit theory showing few research works was performed are available about the design of HP-NGD function [36]–[38].
- Then, very recent studies revealed the design feasibility of the most innovative types of NGD circuits which are classified as SB-NGD function [39], [40]. And deep investigation can be made for this last type of NGD circuit in order to develop some potential applications.

For this reason, the present paper investigates this SB-NGD function and introduces one of its original application for the design of stair phase microwave circuit. The paper is organized in six sections as follows:

- Section II is focused on the unfamiliar SB-NGD topological description. The theoretical approach permitting the SB-NGD topological identification will be introduced.
- Section III develops the S-matrix model of the identified SB-NGD passive cell. The analytical model in function of the RLC-network parameters constituting the unfamiliar SB-NGD cell will be established. The analytical investigation will be followed by the elaboration of the SB-NGD transfer function (TF) canonical form.

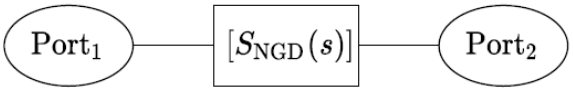

FIGURE 1. Two-port black box of the SB-NGD function.

- In Section IV, the SB-NGD analysis will be developed. Then, the synthesis design equation of circuit in function of the unfamiliar SB-NGD specifications will be formulated.
- Section V is dedicated to the discussion on the unfamiliar SB-NGD function validation results. Comparison between calculated and simulated results of a proof of concept (PoC) will be discussed.
- Section VI is the investigation on the design of stair PS prototype by using the unfamiliar SB-NGD circuit. The design principle of stair PS will be explained. An experimental validation example with a stair unfamiliar PS prototype will be treated.
- Section VII is reserved to the conclusion of the paper.

II. THEORETICAL INVESTIGATION ON UNFAMILIAR SB-NGD CIRCUIT UNDER CONSIDERATION

This section describes the SB-NGD theory. The main specifications of unfamiliar SB-NGD function are defined. The identification approach of the passive topology based on RLC-lumped circuit will be investigated.

A. ANALYTICAL DEFINITION OF SB-NGD FUNCTION

Few research work and studies [39], [40] were made so far on the unfamiliar SB-NGD function. Despite the exiting results available in the literature, the existence of this innovative electronic function remains an open question for most of RF and microwave design, fabrication and test engineers. The present paragraph defines analytically the interpretation of the SB-NGD function. We suppose that the two-port black box microwave symmetric and passive system introduced in Fig. 1 is represented analytically by the S-matrix:

$$[S_{NGD}(s)] = \begin{bmatrix} S_{11}(s) & S_{21}(s) \\ S_{21}(s) & S_{11}(s) \end{bmatrix}. \tag{1}$$

with $s = \omega$ is the Laplace variable expressed in function of angular frequency $\omega = 2\pi f$.

We remind that the magnitude of the reflection and transmission coefficients are given by, respectively:

$$S_{11}(\omega) = |S_{11}(j\omega)| \tag{2}$$

$$S_{21}(\omega) = |S_{21}(j\omega)|. \tag{3}$$

To realize the SB-NGD analysis, the following frequency domain responses are essentially needed:

- the phase of the transmission coefficient which is defined by:

$$\varphi(\omega) = \arg\left[S_{21}(j\omega)\right] \tag{4}$$

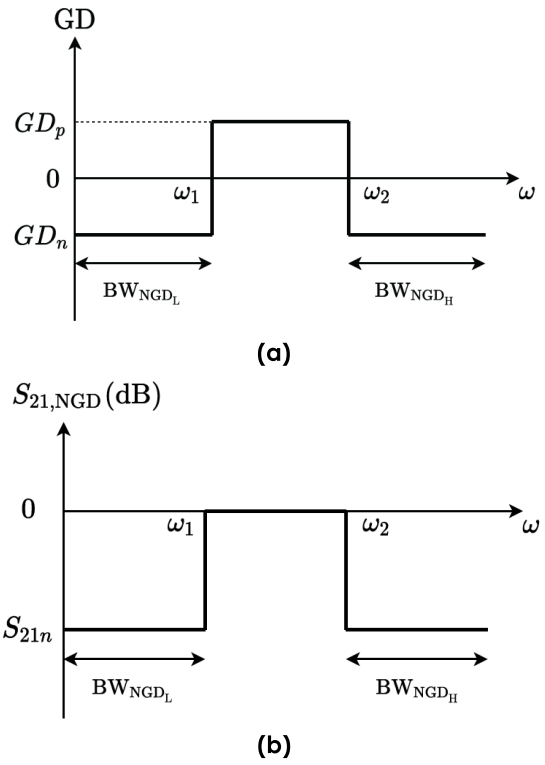

FIGURE 2. (a) GD and (b) transmission coefficient responses of SB-NGD function.

- the frequency dependent GD response which is defined by:

$$GD(\omega) = -\frac{\partial\varphi(\omega)}{\partial\omega}. \tag{5}$$

This system is an NGD function if we can find an angular frequency, ω_x, where:

$$GD(\omega_x) < 0. \tag{6}$$

One of specific types associated to NGD function is the SB-NGD concept. The ideal response of SB-NGD function can be represented by Fig. 2(a) by taking:

- The cut-off angular frequencies, ω_1 and ω_2, as roots of equation:

$$GD(\omega) = 0 \Rightarrow GD(\omega_{1,2}) = 0. \tag{7}$$

- The transmission coefficient ideal response is represented in Fig. 2(b) by:

$$S_{21,NGD}(\omega_1 \leq \omega \leq \omega_2) = 1. \tag{8}$$

In Fig. 2(a) and Fig. 2(b):

- the notation BW_{NGD_L} is used to denote the lower bandwidth,
- and BW_{NGD_H} for higher bandwidth.

Because of its counterintuitive originality, most of non-specialist electronic and RF/microwave engineers confuse the filter and NGD functions. To avoid the misinterpretation, the

following subsection describes the differences between these two electronic functions.

B. SPECIFIC DIFFERENCES BETWEEN SB FILTER AND SB-NGD FUNCTION

The present analytical illustration is based on the consideration of the frequency dependent parameters associated to filter and NGD functions:

- reflection coefficient magnitudes, $S_{11filter}(f)$ and $S_{11NGD}(f)$,
- transmission coefficient magnitudes, $S_{21filter}(f)$ and $S_{21NGD}(f)$,
- and, GDs $GD_{filter}(f)$ and $GD_{NGD}(f)$.

The lower and upper cut-off frequencies in the considered frequency bands are denoted, respectively:

$$\begin{cases} f_1 = \dfrac{\omega_1}{2\pi} \\ f_2 = \dfrac{\omega_2}{2\pi} \end{cases} \tag{9}$$

with $f_1 < f_2$. Thus, the comparison of the SB-NGD and filter behaviors and the associated specification can be made within the frequency band operation bandwidth $f \epsilon [f_1, f_2]$. In brief, the main difference between the classical "stop-band" filter and the "dual-band" NGD filter are based on which parameter is used to describe it. The classical filter uses the magnitude response of the transmission parameter, $|S_{21}(f)|$, while, for instance, in the "stop-band NGD function", it is defined by the NGD frequency band where the group delay meets the condition $GD(f) < 0$ [34]. Different parameters related to the maximum GD of the filter and the maximum attenuation of NGD must be considered to characterize the functions.

To illustrate the identification of SB NGD topology, a general analytical approach will be elaborated in the following subsection.

C. IDENTIFICATION APPROACH OF SB-NGD TOPOLOGY

The identification approach of SB-NGD topology can be made by the analogy with the filter [34]. Substantially, we have identified the SB-NGD passive circuit from the low-pass (LP) NGD cell based on L-inductance. The elaboration of SB-NGD cell can be made from the equivalent impedance given by:

$$Z_a(s) = Ls. \tag{10}$$

as the reactive element. As reported in [35] and [36], the passive cell constituted by an RL-series network mounted in parallel behaves as a LP-NGD first-order circuit presented in Fig. 3.

We can identify from this LP-NGD cell, the SB-NGD family by substituting the inductance L by an LC-parallel network. It yields the two-port circuit represented by the SB-NGD topology shown in Fig. 4. It acts as a second order circuit.

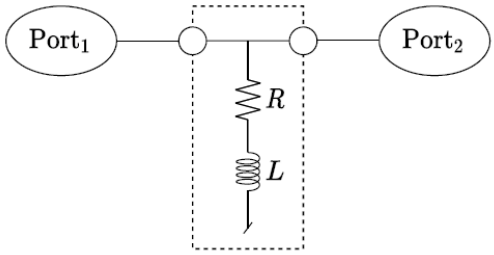

FIGURE 3. LP-NGD cell.

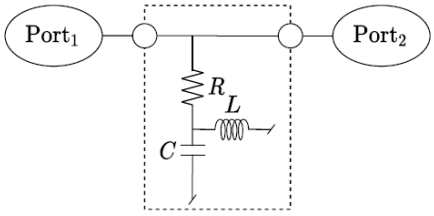

FIGURE 4. SB-NGD cell inspired in the family of the LP-NGD cell shown in Fig. 3.

For this case, the equivalent impedance is given by:

$$Z_b(s) = \frac{Ls}{1 + LCs^2}. \tag{11}$$

To analyze the identified SB-NGD cell, the S-matrix model is elaborated in the following section.

III. S-MATRIX MODEL AND TRANSFER FUNCTION (TF) CANONICAL FORM OF THE SB-NGD TOPOLOGY

Similar to classical RF and microwave circuits, the theoretical analysis of the unfamiliar SB-NGD circuit will be based on the equivalent S-matrix model. Then, the SB-NGD canonical form will be established before the design equation formulation.

The S-matrix modelling of the SB-NGD topology under study will be described in the following paragraph.

A. S-MATRIX MODEL OF THE SB-NGD TOPOLOGY

Let us take the terminal reference impedance, $R_0 = 50\ \Omega$. We can demonstrate analytically that the impedance matrix of the SB-NGD topology shown in Fig. 3 is written as:

$$[Z(s)] = \begin{bmatrix} R + Z_b(s) & R + Z_b(s) \\ R + Z_b(s) & R + Z_b(s) \end{bmatrix}. \tag{12}$$

According to the circuit and system theory, the associated S-matrix, introduced in equation (1), can be calculated from Z-to-S transform:

$$[S_{NGD}(s)] = \left\{ \begin{array}{l} \left([Z(s)] - \begin{bmatrix} R_0 & 0 \\ 0 & R_0 \end{bmatrix} \right) \times \\ \left([Z(s)] + \begin{bmatrix} R_0 & 0 \\ 0 & R_0 \end{bmatrix} \right)^{-1} \end{array} \right\}. \tag{13}$$

Therefore, we establish the reflection and transmission coefficients, respectively, as:

$$S_{11}(s)=S_{22}(s)=\frac{-R_0(1+LCs^2)}{2R+R_0+2Ls+LC(2R+R_0)s^2} \quad (14)$$

$$S_{21}(s)=S_{12}(s)=\frac{2(R+Ls+RLCs^2)}{2R+R_0+2Ls+LC(2R+R_0)s^2}. \quad (15)$$

The corresponding SB-NGD analysis is mainly focused on the last expression as described in the next paragraph.

B. CANONICAL FORM OF SB-NGD TF

The TF associated to the SB-NGD topology is generally represented by the transmission coefficient:

$$T(s)=S_{21}(s). \quad (16)$$

Let us denote the center angular frequency of the positive GD (PGD) as:

$$\omega_0=2\pi f_0 \quad (17)$$

where:

$$T(\omega=\omega_0)=|S_{21}(j\omega)|_{\omega=\omega_0}=1. \quad (18)$$

Then, we denote also the following NGD key parameters, GD value and the transmission coefficient, respectively:

$$\tau_n = GD(\omega_0) \quad (19)$$

$$T_n = |S_{21}(j\omega)|_{\omega=0}=S_{21}(\omega=0). \quad (20)$$

With the real positive parameter, $T_n < 1$, the SB-NGD TF canonical form can be expressed as:

$$T(s)=\frac{T_n(s^2+\omega_a s+\omega_0^2)}{s^2+\omega_b s+\omega_0^2} \quad (21)$$

where:

$$\omega_a = \frac{2(1-T_n)}{T_n\tau_n} \quad (22)$$

$$\omega_b = \frac{2(1-T_n)}{\tau_n}. \quad (23)$$

By identification with the transmission coefficient expressed in equation (15), we have:

$$T_n = \frac{2R}{2R+R_0} \quad (24)$$

$$\omega_0 = \frac{1}{\sqrt{LC}} \quad (25)$$

$$\tau_n = R_0C=\frac{R_0}{L\omega_n^2}>0. \quad (26)$$

In this case, the reflection coefficient proposed in equation (14) can then be rewritten as:

$$S_{11}(s)=\frac{(T_n-1)(s^2+\omega_0^2)}{s^2+\omega_b s+\omega_0^2}. \quad (27)$$

Knowing the S-matrix model, the frequency responses will be analyzed in the following subsection.

C. ANALYSIS OF S-PARAMETER FREQUENCY RESPONSES

The magnitudes of the reflection and transmission coefficients, $S_{11}(\omega)=|S_{11}(j\omega)|$ and $T(\omega)=|T(j\omega)|$ are given, respectively, by:

$$S_{11}(\omega)=\frac{\left|(1-T_n)(\omega^2-\omega_0^2)\right|}{\sqrt{\tau_n^2(\omega^2-\omega_0^2)^2+4(\omega-T_n\omega_0)^2}} \quad (28)$$

$$T(\omega)=\frac{\sqrt{(T_n\tau_n)^2(\omega^2-\omega_0^2)^2+4(\omega-T_n\omega_0)^2}}{\sqrt{\tau_n^2(\omega^2-\omega_0^2)^2+4(\omega-T_n\omega_0)^2}}. \quad (29)$$

The transmission phase yielded from the transmission coefficient is expressed as:

$$\varphi(\omega)=\varphi_{\varpi}(\omega)-\varphi_{\vartheta}(\omega) \quad (30)$$

with:

$$\varphi_{\varpi}(\omega)=\arctan\left[\frac{2(T_n-1)\omega}{T_n\tau_n(\omega^2-\omega_0^2)}\right] \quad (31)$$

and:

$$\varphi_{\vartheta}(\omega)=\arctan\left[\frac{2(1-T_n)\omega}{\tau_n(\omega^2-\omega_0^2)}\right]. \quad (32)$$

The SB-NGD analysis can be explored from these expressions.

IV. SB-NGD ANALYSIS AND SYNTHESIS OF THE IDENTIFIED RLC-NETWORK BASED TOPOLOGY

The NGD analysis consists in the identification of the NGD existence condition written in equation (6), in the appropriated frequency bands. The NGD condition can be transformed into a relation between the elements of the topology under study by considering the GD expressed in equation (5). Subsequently, to explore this condition, we need to start with the GD expression versus frequency.

A. FREQUENCY DEPENDENT EXPRESSION OF GD

The GD defined in equation (5), which takes into account the transmission phase written in equation (30), is expressed as:

$$GD(\omega)=GD_{\vartheta}(\omega)-GD_{\varpi}(\omega) \quad (33)$$

or

$$GD(\omega)=\frac{\partial\varphi_{\vartheta}(\omega)}{\partial\omega}-\frac{\partial\varphi_{\varpi}(\omega)}{\partial\omega} \quad (34)$$

with

$$GD_{\varpi}(\omega)=\frac{2\tau_n(1-T_n)(\omega^2+\omega_0^2)}{\tau_n^2(\omega^4+\omega_0^4)+2\left[2(1-T_n)^2-\tau_n^2\omega_0^2\right]\omega^2} \quad (35)$$

$$GD_{\vartheta}(\omega)=\frac{2\tau_nT_n(T_n-1)(\omega^2+\omega_0^2)}{T_n^2\tau_n^2(\omega^4+\omega_0^4)+2\left[2(1-T_n)^2-T_n^2\tau_n^2\omega_0^2\right]\omega^2} \quad (36)$$

The exploration of this GD constitutes the SB-NGD analysis and synthesis to be developed in the next subsection.

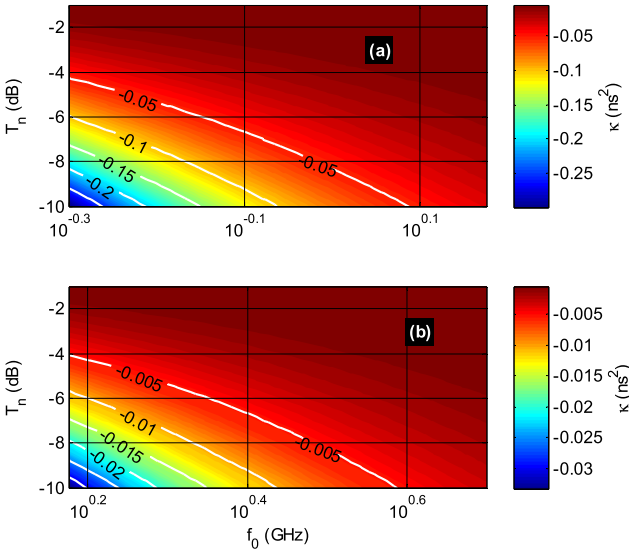

FIGURE 5. Product κ versus (f_n, T_n) with f_n (a) from 0.5 to 1.5 GHz and (b) from 1.5 GHz to 5 GHz.

B. ANALYSIS AT VERY LOW FREQUENCIES ($\omega \approx 0$)

We recall that at very low frequencies, $\omega \approx 0$, the reflection and transmission coefficients of equations (28) and (29) become:

$$\begin{cases} S_{11}(\omega = 0) = 1 - T_n \\ S_{21}(\omega = 0) = T_n \end{cases} \tag{37}$$

At the same frequency, the GD introduced in equation (31) is simplified as:

$$GD(\omega \approx 0) = \frac{-2(1 - T_n)^2}{T_n \tau_n \omega_0^2} < 0. \tag{38}$$

For the interpretation of this relation, the mapping of the product:

$$\kappa = GD(f \approx 0) \times GD(f \approx f_0) \tag{39}$$

versus (f_0, T_n) varied from (0.5 GHz, −10 dB) to (5 GHz, −1 dB) is presented in Figs. 5. It can be seen that the product κ is inversely proportional to f_n and T_n. As an interesting remark inferred from the plot of Figs. 5:

- when f_n increases from 0.5 GHz to 1.5 GHz, the product, κ, decreases from about −0.3 ns^2 to −299 ps^2,
- and when the characteristic frequency varies from 1.5 GHz to 5 GHz, the product, κ, decreases from −0.03 ns^2 to −26.9 ps^2.

C. EXPRESSION OF SB-NGD BANDWIDTH

We can remark that the GD established in equation (38) is always negative for any values of parameters in the topology proposed in Fig. 4. Moreover, the NGD cut-off frequencies can be determined as the roots of equation (7) by using the GD given in (33). Consequently, we find the cut-off frequencies given by:

$$\omega_1 = \frac{\sqrt{2(T_n - 1)^2 + T_n(\tau_n\omega_0)^2 + 2\zeta(1 - T_n)}}{\tau_n\sqrt{T_n}} \tag{40}$$

$$\omega_2 = \frac{\sqrt{2(T_n - 1)^2 + T_n(\tau_n\omega_0)^2 - 2\zeta(1 - T_n)}}{\tau_n\sqrt{T_n}} \tag{41}$$

where:

$$\zeta = \sqrt{(T_n - 1)^2 + T_n(\tau_n\omega_0)^2}. \tag{42}$$

The bandwidth with positive GD (PGD) can be calculated with the relation:

$$BW = \omega_2 - \omega_1. \tag{43}$$

D. PROPERTIES OF SB-NGD FUNCTION

Similar to the cases of the most developed types of NGD function as LP-NGD and BP-NGD ones, the SB-NGD function presents some specific analytical properties. It is interesting to note that the cut-off frequencies and PGD center frequency are linked by the equation:

$$\frac{\omega_2\omega_1}{\omega_0^2} = 1. \tag{44}$$

In addition to this relationship, we remind also that:

- At the central frequency According to equation (18), the magnitude $T(\omega = \omega_0) = 1$ and the GD at the is equal to $GD(\omega_0) = \tau_n > 0$.
- At very low frequency, the magnitude as given in equation (35) must be $T(\omega \approx 0) < 1$ and the GD at very low frequency $GD(\omega \approx 0) < 0$.

In brief, the passive circuit introduced in Fig. 4 enables to have:

$$\begin{cases} GD(\omega < \omega_1) < 0 \\ GD(\omega_1 < \omega < \omega_2) > 0 \\ GD(\omega > \omega_2) < 0 \end{cases} \tag{45}$$

This statement confirms that the circuit introduced in Fig. 4 behaves as a SB-NGD function.

E. SYNTHESIS AND DESIGN EQUATIONS OF SB-NGD CIRCUIT

The design of the SB-NGD circuit must start with the specifications of:

- The PGD center frequency, τ_n,
- The attenuation at very low frequency, T_n,
- The expected PGD, τ_n, which is linked with the NGD at very low frequency, $\tau_0 = GD_0 < 0$, given in equation (36).

Therefore, the equations of the SB-NGD circuit R, L, and C parameters are given by:

$$R = \frac{T_n R_0}{2(1 - T_n)} \tag{46}$$

$$L = \frac{R_0}{\tau_n \omega_0^2} \tag{47}$$

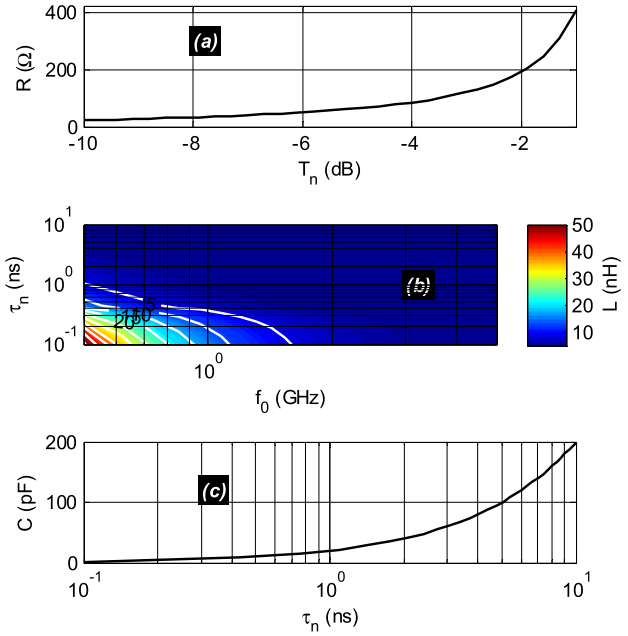

FIGURE 6. Variations of SB-NGD circuit parameters: (a) R, (b) L, and (c) C, versus (T_n, τ_n).

TABLE 2. Minimum and maximum values of synthesized *R*, *L* and *C* parameters.

Parameters	T_n	τ_n	R	L	C
Min.	-10 dB	0.1 ns	23.1 Ω	5.1 pH	2 pF
Max.	-1 dB	10 ns	410 Ω	50.7 nH	0.2 nF

$$C = \frac{\tau_n}{R_0}. \tag{48}$$

We can remind that T_n must verify the condition, $0 < T_n < 1$. The different ranges of R, L, and C values versus (T_n, τ_n) are plotted in Figs. 6. According to these graphical plots, it can be seen that:

- R increases with T_n, L varies inversely proportional to T_n and τ_n, and C increases proportionally to τ_n.
- The R-variation slope is particularly weak, lower than 10 Ω/dB, when T_n is below −6 dB, against the slope above −4 dB, which is more than 100 Ω/dB.
- The C-variation presents a slope less than 10 pF/decade when τ_n is lower than 1 ns against more than 100 pF/decade when τ_n is higher than 1 ns.

Table 2 summarizes the minimal and maximal values of R, L, and C versus the considered minimal and maximal range of (T_n, τ_n).

To verify the feasibility of the developed SB-NGD theory, PoC practical investigation will be presented in the next section.

V. VERIFICATION RESULTS WITH PROOF OF CONCEPT (POC) CIRCUIT OF SB-NGD TOPOLOGY

The present section deals with the validations of the SB-NGD topology. After the PoC description, parametric simulations are described in order to quantify the influence of the R, L, and C component parameters on the NGD behavior. The overall validation aspects are originally focused on analyzing NGD function.

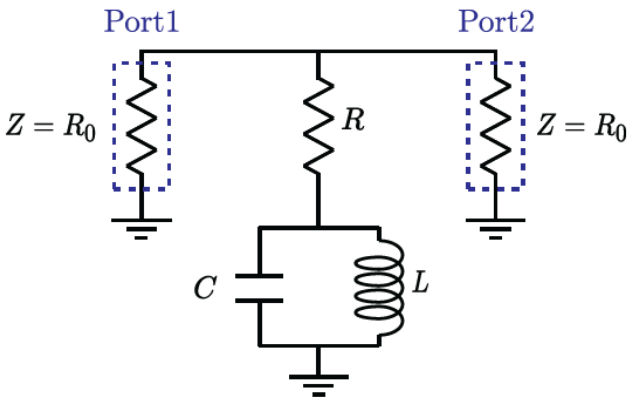

FIGURE 7. Schematic of the simulated SB-NGD circuit PoC.

TABLE 3. Parameters of the SB-NGD circuit PoC.

Description	Parameter	Ideal value
Specifications	Center frequency	f_0=2.45 GHz
	BW	BW_{PGD}=0.3 GHz
	NGD value	τ_n=-0.1 ns
	Attenuation	T_0=-3 dB
Calculated NGD circuit parameters	Resistor	R=61 Ω
	Inductor	L=0.5 nH
	Capacitor	C=8.35 pF

A. POC DESIGN DESCRIPTION

The SB-NGD circuit design was performed with the application of synthesis equations of R, L, and C expressed in equations (46), (47), and (48), respectively. Fig. 7 shows the design of the SB-NGD schematic circuit in the environment of the electronic and RF/microwave circuit simulator ADS® from Keysight Technologies. The NGD specifications and designed circuit electrical parameters are indicated in Table 3.

To illustrate the robustness of the SB-NGD behavior, sensitivity analysis with respect to the circuit parameters will be discussed in the following subsection.

B. SB-NGD RESPONSE SENSITIVITY ANALYSIS

Sensitivity analyses with respect to the resistor, R+/−5%, inductor, L+/−5%, and capacitor, C+/−5%, have been conducted for the robustness of the SB-NGD circuit. The sensitivity analyses enable to explain more explicitly the circuit parameter effects onto the SB-NGD function. The MATLAB® calculations of GD, S_{11}, and S_{21} introduced in equation (33), equation (28), and equation (29) to be discussed in the following paragraphs with the S-parameter analytical expressions, are carried out from 2 GHz to 3 GHz.

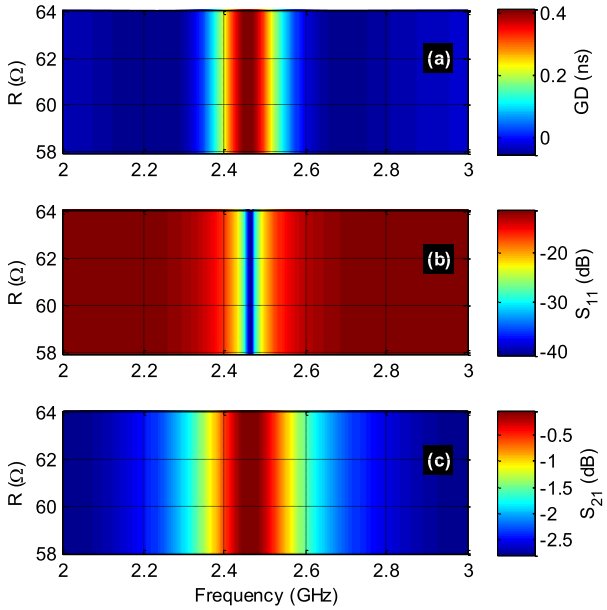

FIGURE 8. Parametric results versus R: (a) GD, (b) S_{11}, and (c) S_{21}.

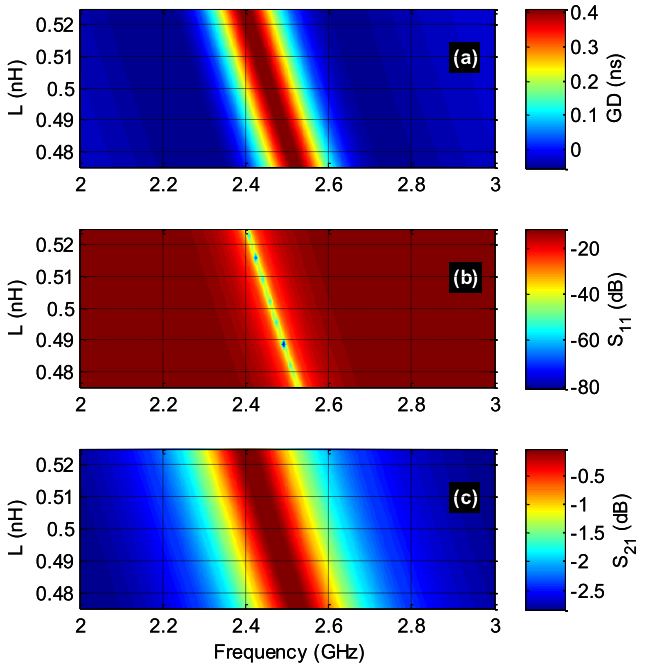

FIGURE 9. Parametric results versus L: (a) GD, (b) S_{11}, and (c) S_{21}.

1) SENSITIVITY ANALYSIS VERSUS R

The effect of resistor, R, was investigated under linear variations from 58 Ω to 64 Ω with τ fixed values of L and C. The calculated results are represented as cartographies with color scale variation of responses in function of couple (f_0, R). Fig. 8(a), Fig. 8(b), and Fig. 8(c) display the results of the calculations of GD, S_{11}, and S_{21}, respectively. The SB-NGD behavior is occurred for all the value of the considered range of R. It is noteworthy that the specified parameters, center frequency, $f_0 = 2.458$ GHz, $GD(f_0) = 0.42$ ns, $S_{11}(f_0) = -38$ dB, and $S_{21}(f_0) = -4$ mdB are less sensitive to variation of R.

2) SENSITIVITY ANALYSIS VERSUS L

The inductor variation effect was investigated via linear sensitivity analysis of inductor L varied from 4.75 nH to 5.25 nH with fixed resistor and capacitor during the S-parameter calculations. Fig. 9(a), Fig. 9(b), and Fig. 9(c) display the corresponding results.

It can be seen with the three cartographies that the NGD center frequency increases with L. More rigorous analysis can be done from observation of f_0, $GD(f_0)$, $S_{11}(f_0)$, and $S_{21}(f_0)$ variations plotted in Figs. 10(a), Fig. 10(b), and Fig. 10(c), respectively.

3) SENSITIVITY ANALYSIS VERSUS C

This paragraph presents the capacitor variation effect onto the SB-NGD circuit responses.

The analysis is performed with linear sensitivity analysis of capacitor C varied from 7.93 pF to 8.77 pF with fixed resistor and inductor during the S-parameter calculations. Fig. 11(a), Fig. 11(b), and Fig. 11(c) display the corresponding results. It can be seen with the three cartographies that the NGD

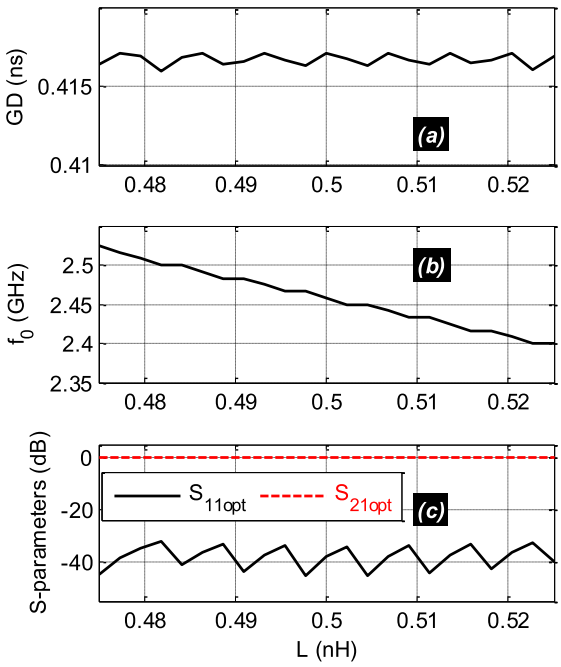

FIGURE 10. GD(f_0), f_0, $S_{11}(f_0)$, and $S_{21}(f_0)$ versus L.

center frequency increases with C. More rigorous observation of f_0 increasing from 2.4 GHz to 2.525 GHz, $GD(f_0)$, $S_{11}(f_0)$, and $S_{21}(f_0)$ variations are plotted in Fig. 12(a), Fig. 12(b), and Fig. 12(c), respectively.

C. DISCUSSION ON CALCULATED AND SIMULATED SB-NGD RESULTS

The PoC of SB-NGD circuit was simulated from 2 GHz to 3 GHz. Comparisons between the calculated (“Calc.”) and simulated (“Simu.”) with ADS® results are displayed in

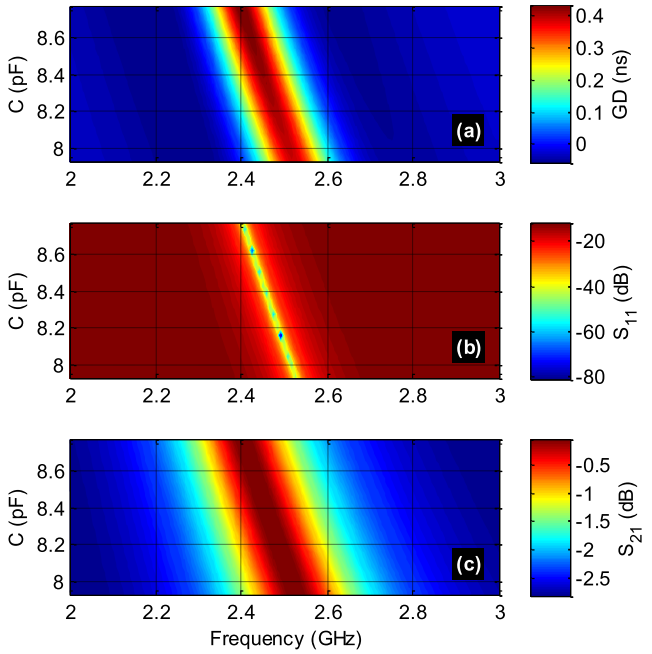

FIGURE 11. Parametric results versus C: (a) GD, (b) S_{11}, and (c) S_{21}.

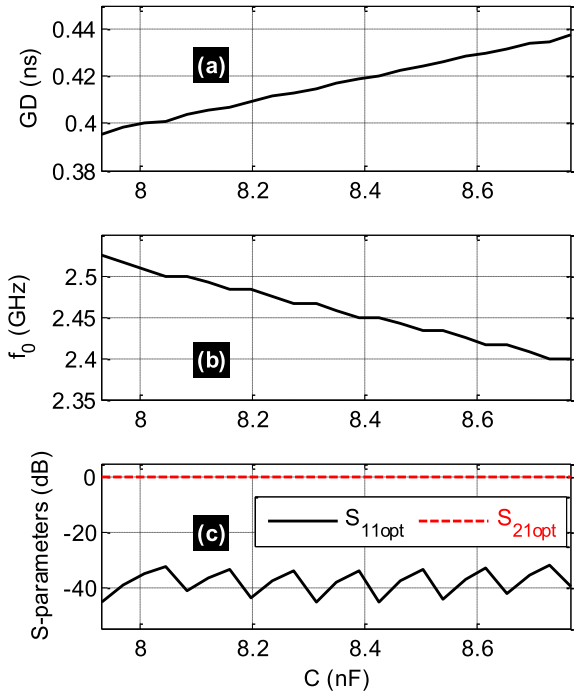

FIGURE 12. GD(f_0), f_0, $S_{11}(f_0)$, and $S_{21}(f_0)$ versus C.

Fig. 13. The calculated results were obtained with a program developed in Matlab using S-parameters equations. It can be pointed out that these comparative results present a very good agreement. As expected, and seen in Fig. 13(a), in the working frequency band, the considered circuit PoC presents a SB-NGD behavior around center frequency of approximately $f_0 = 2.46$ GHz.

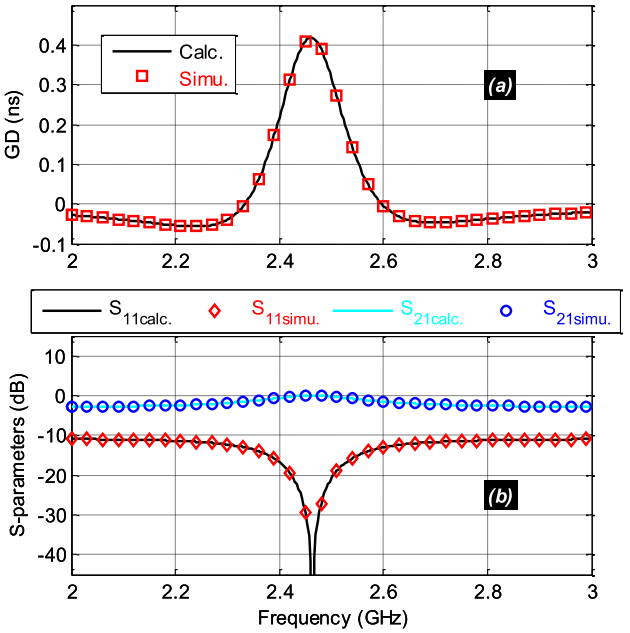

FIGURE 13. Comparisons of calculated and simulated (a) GD and (b) transmission parameters from the SB-NGD PoC shown in Fig. 8.

TABLE 4. Comparison of calculated and simulated SB-NGD prototype parameters.

Approach	f_o (GHz)	$\tau(f_o)$ (ns)	BW (MHz)	$S_{21}(f_o)$ (dB)	$S_{11}(f_o)$ (dB)
Calculated	2.46	4.17	267	-0.42	-17
Simulated	2.46	4.16	268	-0.41	-18

TABLE 5. Comparison of SB NGD circuit specifications with the state-of-the-art.

Approach	f_o	$\tau(f_o)$	BW	Attenuation @ f_o
[36]	0.5 GHz	2 ns	46 MHz	-0.05 dB
[39]	32 MHz	0.89 ns	83.6 MHz	-7.3 dB
[40]	0.95 kHz	108 µs	1.45 kHz	-4.08 dB
This work	2.46 GHz	4.16 ns	268 MHz	-0.41 dB

Table 4 summarizes the differences between the calculated and simulated NGD parameters.

After the SB-NGD sensitivity analysis and feasibility study, an original case of application to design a stair PS for microwave system will be explored in the following section.

D. COMPARISON OF SB NGD SPECIFICATIONS

The present subsection proposes a state-of-the-art investigation about the unfamiliar SB NGD function. We can compare the specifications of the considered NGD circuit with the very few research works available in the literature about the SB NGD circuit design [36], [39], [40]. Table 5 summarizes the comparison of NGD at center frequency f_o, GD $\tau(f_o)$ at the center frequency, bandwidth BW and also the attenuation at center frequency.

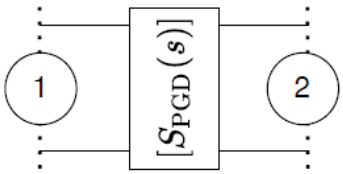

FIGURE 14. Two-port black box of positive group delay (PGD) circuit.

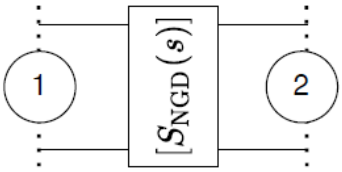

FIGURE 15. Two-port black box of NGD ideal circuit.

The present research work is particularly challenging with the possibility of SB-NGD circuit design operating at higher central frequency with very low attenuation loss.

At this stage, we may wonder about the designability of SB NGD integrating into a PS. The following section develops the innovative stair PS design, fabrication and test of the proof of concept.

VI. SB-NGD CIRCUIT BASED-STAIR PS DESIGN, FABRICATION AND TEST

As original application of the previously investigated SB-NGD circuit, we can design an innovative stair PS never been done before. The next paragraph introduces the principle of the stair PS.

A. THEORETICAL APPROACH OF STAIR PS DESIGNING

The present subsection describes the theoretical approach of SB-NGD function application for stair PS circuit design. The design is illustrated by graphical diagram representation based on the S-matrix operation.

1) DESIGN PRINCIPLE OF STAIR PS WITH SB-NGD FUNCTION

For the basic understanding, we consider the case of two-step stair PS in the present study. Thus, we assume that the frequency band of interest is written as:

$$BW_L = \left[\omega_{L_1}, \omega_{L_2}\right]. \tag{49}$$

The original stair PS under study is ontologically implemented with cascade of ideal PGD and NGD two-port circuits as introduced in [22]–[24] for the case of BP-NGD circuit. To illustrate the ideal principle elaborated in the present subsection, we suppose that the reflection coefficients of the ideal PGD and NGD two-port circuits are negligible:

$$\left|S_{11,22,PGD}(j\omega)\right| = \left|S_{11,22,NGD}(j\omega)\right| = 0. \tag{50}$$

The NGD-function based PS explored in [22]–[24] is specified by the phase shift value independent to the frequency on the band of interest. To obtain such a particular behavior, the PGD and NGD circuits must fulfil certain specific requirements as introduced in the following paragraphs.

2) IDEAL SPECIFICATION OF PGD BLOCK OF THE NGD-PS CIRCUIT

The ideal specification of the PGD block is defined by the analytical approach by assuming with the constant (independent of frequency) ideal GD value:

$$GD_{PGD}(\omega) = \tau_a > 0. \tag{51}$$

Figs. 14 represents the S-matrix block of the perfectly access matched PGD as a two-port circuit which means:

$$S_{11,PGD}(j\omega) = S_{22,PGD}(j\omega) \approx 0. \tag{52}$$

Therefore, the corresponding S-matrix can be expressed by the ideal equations:

$$[S_{PGD}(j\omega)] = \begin{bmatrix} 0 & S_{21,PGD}(j\omega) \\ S_{21,PGD}(j\omega) & 0 \end{bmatrix} \tag{53}$$

knowing that:

$$S_{21,PGD}(j\omega) = S_a \exp\left[j(\varphi_a - \omega\tau_a)\right] \tag{54}$$

with the constant phase, φ_a, and constant magnitude:

$$\left|S_{21,PGD}(j\omega)\right| = S_a < 1. \tag{55}$$

The NGD block must operate in opposite phase of the PGD one. The NGD block ideal specification will be defined in the following paragraph.

3) IDEAL SPECIFICATION OF NGD BLOCK OF THE NGD-PS CIRCUIT

In this case, let us denote the ideal GD value of NGD block as:

$$GD_{NGD}(\omega) = \tau_b < 0. \tag{56}$$

The NGD circuit is assumed with constant magnitude:

$$\left|S_{21,NGD}(j\omega)\right| = S_b < 1 \tag{57}$$

and constant phase:

$$\arg\left[S_{21,NGD}(j\omega)\right] = \varphi_b. \tag{58}$$

Figs. 15 represents the S-matrix blocks of the perfectly access matched NGD system modelled by the ideal equation:

$$[S_{NGD}(j\omega)] = \begin{bmatrix} 0 & S_{21,NGD}(j\omega) \\ S_{21,NGD}(j\omega) & 0 \end{bmatrix} \tag{59}$$

where:

$$S_{21,NGD}(j\omega) = S_b \exp\left[j(\varphi_b - \omega\tau_b)\right]. \tag{60}$$

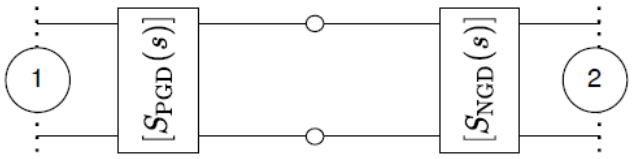

FIGURE 16. Two-port black box of frequency-independent PS constituted by PGD and NGD ideal circuits in cascade.

4) IDEAL REPRESENTATION OF STAIR PS WITH SB-NGD FUNCTION

The associated block is illustrated by the diagram of Fig. 16. Since the reflection coefficients are negligible as defined by equation (50), it should present the S-matrix product as

$$[S_{PS}(j\omega)] = [S_{PGD}(j\omega)] \times [S_{NGD}(j\omega)]\,. \tag{61}$$

By means of 2-D matrices introduced in equation (52) and equation (59), we have the ideal expression of PS S-matrix model:

$$[S_{PS}(j\omega)] = \begin{bmatrix} 0 & S_{21,PS}(j\omega) \\ S_{21,PS}(j\omega) & 0 \end{bmatrix} \tag{62}$$

with

$$S_{21,PS}(j\omega) = S_a S_b \exp\{j\,[\varphi_b + \varphi_b - \omega(\tau_a + \tau_b)]\}\,. \tag{63}$$

In the frequency band of the study, we can realize a frequency independent PS as illustrated by Fig. 17(a) by choosing the GD proposed in Fig. 17(b):

$$GD_{NGD}(\omega) = -GD_{PGD}(\omega). \tag{64}$$

Therefore, it means that we should have:

$$\tau_b = -\tau_a. \tag{65}$$

The PGD and NGD associated frequency dependent phase values are given by, respectively:

$$\begin{cases} \varphi_{21,PGD}(\omega) = \arg\left[S_{21,PGD}(j\omega)\right] = \varphi_{21,PGD}(\omega_{L_1}) - \omega\tau_a \\ \varphi_{21,NGD}(\omega) = \arg\left[S_{21,NGD}(j\omega)\right] = \varphi_{21,NGD}(\omega_{L_1}) - \omega\tau_b \end{cases} \tag{66}$$

5) IDEAL VALUES OF PHASE SHIFT AND GD IN THE EACH FREQUENCY BAND OF STAIR STEPS

The consideration of the dual-band NGD aspect related to the SB-NGD function as BW_L and BW_H shown in Fig. 18(a), enables to generate a two-step stair PS:

$$\begin{cases} \varphi(\omega_{L_1} \le \omega \le \omega_{L_2}) = \varphi_1 \\ \varphi(\omega_{L_2} \le \omega \le \omega_{H_1}) = \varphi_1 - \omega\tau_2 \\ \varphi(\omega_{H_1} \le \omega \le \omega_{H_2}) = \varphi_2 \end{cases} \tag{67}$$

with:

$$\begin{cases} \varphi_1 = \varphi(\omega_{L_1}) = -\omega\tau_1 \\ \varphi_2 = \varphi(\omega_{H_1}) = -\omega\tau_3 + \varphi_1 \end{cases} \tag{68}$$

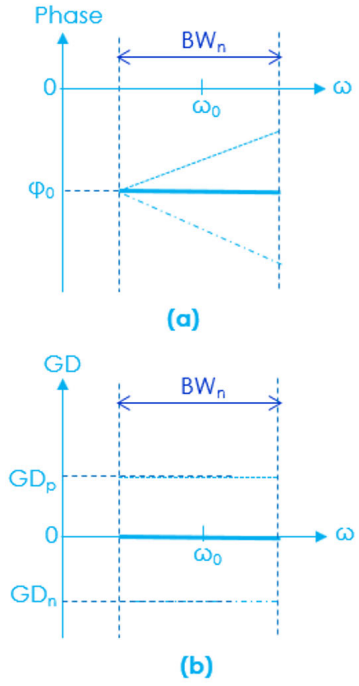

FIGURE 17. (a) Phase and (b) GD responses of PGD, NGD, and frequency-independent PS.

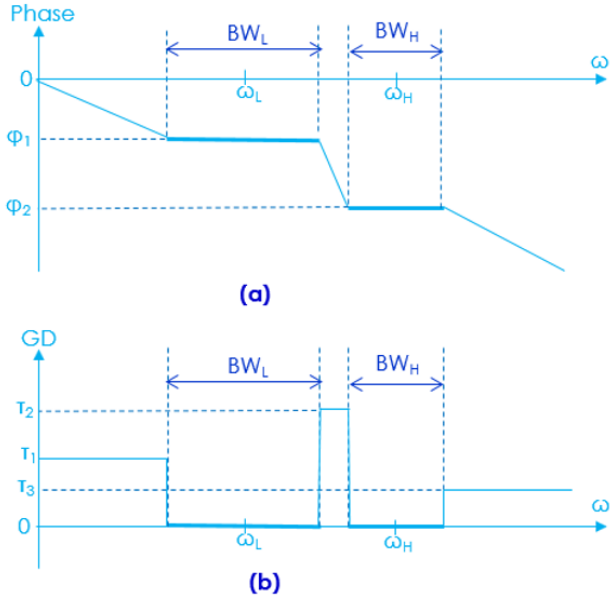

FIGURE 18. (a) Phase and (b) GD ideal responses of two-step stair PS.

In this case, the GD response can be represented as shown in Fig. 18(b), which is defined as:

$$\begin{cases} GD(\omega \le \omega_{x1}) = \tau_1 \\ GD(\omega_{x1} \le \omega \le \omega_{x2}) = \tau_2 \\ GD(\omega_{x2} \le \omega \le \omega_{y1}) = \tau_3 \\ GD(\omega_{y1} \le \omega \le \omega_{y2}) = \tau_2 \end{cases} \tag{69}$$

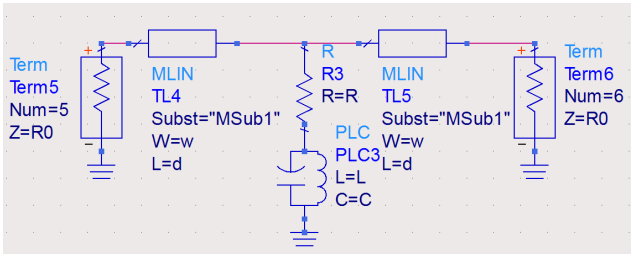

FIGURE 19. Schematic of the designed stair PS prototype.

To validate the feasibility of the introduced ideal principle, a prototype of stair PS circuit PoC will be investigated in the following subsection.

B. STAIR PS DESIGN AND MODELLING WITH DISTRIBUTED SB-NGD CIRCUIT

The design of the stair PS is explored in the present subsection. The design is based on the SB-NGD microstrip distributed circuit. The equivalent model between lumped and distributed inductor and capacitor will be proposed.

1) DESCRIPTION OF THE DESIGNED PROTOTYPE OF STAIR PS POC

To validate the applicative concept, the developed SB-NGD function was used to design a stair PS. The prototype of stair PS circuit PoC was designed in hybrid technology. The PS consists of cascaded PGD constituted by TL and the SB-NGD circuit. The TL was implemented in microstrip technology with physical width, w, and physical total length, d. Fig. 19 represents the schematic of the stair PS PoC designed in the environment of the ADS® electronic and RF/microwave simulation tools from Keysight technologies®.

First, a ''lumped'' PS circuit was designed and simulated with the SB-NGD specified in Table 2. However, the small values of inductor and capacitor are not available in our laboratory. Therefore, a ''distributed'' PS circuit was designed on Isola Astra 3 dielectric substrate with a surface mounted component (SMC) resistor. The following paragraph will propose the used distributed model of inductor and capacitor.

2) MODEL OF MICROSTRIP DISTRIBUTED INDUCTOR AND CAPACITOR

The distributed microstrip structures, inductance and capacitance, widths and lengths are denoted by (w_{ind}, d_{ind}) and (w_{cap}, d_{cap}), respectively. During the design phase, we have considered the following constants:

- the effective permittivity, ε_{reff},
- the center angular frequency, $\omega_0 = 2\pi f_0$,
- $Z_c(w_{ind})$ and $Z_c(w_{cap})$ are the inductor element characteristic impedances,
- and c is the vacuum light speed.

According to the TL theory, the lumped inductor component can be estimated from the distributed physical parameters by the formula:

$$L = \frac{Z_c(w_{ind})\tan(\theta_{ind})}{\omega_0} \tag{70}$$

with the electrical angle:

$$\theta_{ind} = \frac{\omega_0 d_{ind}\sqrt{\varepsilon_{reff}}}{c}. \tag{71}$$

Under the similar approach, the capacitor component can be estimated from the formula:

$$C = \frac{\tan(\theta_{cap})}{\omega_0 Z_c(w_{cap})} \tag{72}$$

with:

$$\theta_{cap} = \frac{\omega_0 d_{cap}\sqrt{\varepsilon_{reff}}}{c}. \tag{73}$$

By choosing the electrical angle respecting the condition, we can assume that $\tan(\theta_{ind}) \approx \theta_{ind}$ and $\tan(\theta_{cap}) \approx \theta_{cap}$. Consequently, we can estimate the inductor and capacitor formulas introduced in equation (70) and equation (72) as:

$$L \approx \frac{Z_c(w_{ind})d_{ind}\sqrt{\varepsilon_{reff}}}{c} \tag{74}$$

$$C \approx \frac{d_{cap}\sqrt{\varepsilon_{reff}}}{cZ_c(w_{cap})}. \tag{75}$$

After estimation of the distributed components, the designed stair PS was fabricated. The results are discussed in the following subsection.

C. STAIR PS PROTOTYPING AND EXPERIMENTAL VALIDATION RESULTS

The present subsection is focused on the discussion on the successfully fabricated two-step stair PS and also the experimented validation results. Comparisons of results obtained from calculations, simulation with the ADS® electronic and RF/microwave simulation tools from Keysight technologies®, and measurements are discussed.

1) DESCRIPTION OF THE FABRICATED PROTOTYPE OF STAIR PS POC

Based on the previously introduced formulas of distributed self-inductor and capacitor, a prototype of hybrid and microstrip circuit was designed, fabricated and tested. The microstrip specifications of substrate susceptible to operate in the expected frequency band of interest are determined. The substrate physical characteristics are addressed in Table 6. The distributed stair PS circuit was implemented.

The layout of the stair PS prototype is shown by Fig. 20(a). The top and bottom view photographs of the fabricated PS prototype are displayed in Fig. 20(b) and Fig. 20(c). This stair PS circuit prototype was tested to extract the measured S-parameter. The following paragraph describes the obtained results.

TABLE 6. Physical parameters of the substrate used in the stair PS circuit.

Structure	Description	Parameters	Values
Substrate	Relative permittivity	ε_r	3
	Loss tangent	$\tan(\delta)$	0.0017
	Thickness	h	0.76 mm
Metallization conductor	Copper conductivity	σ	58 MS/s
	Thickness	t	35 µm
Access line	Length	d	2×9 mm
	Width	w	1.53 mm
	Propagation delay	τ_p	91.2 ps
SMD component	Resistor	R	62 Ω
Distributed inductance structure	Length	d_{ind}	5.53 mm
	Width	w_{ind}	6.4 mm
Distributed capacitance structure	Length	d_{cap}	12 mm
	Width	w_{cap}	5 mm

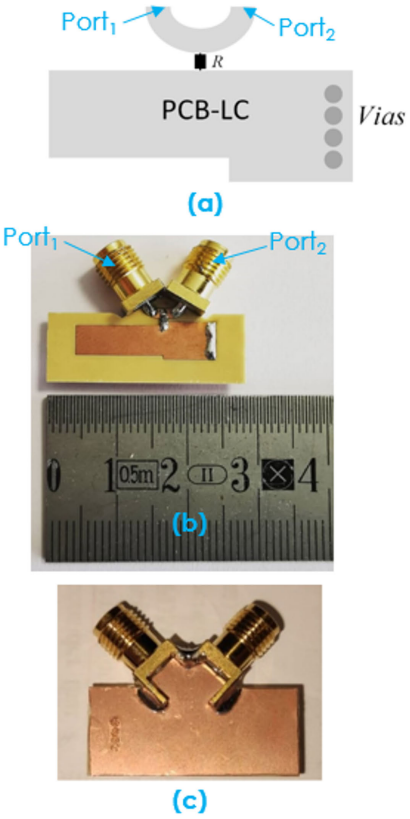

FIGURE 20. (a) Layout, (b) top and (c) bottom view photographs of the fabricated stair PS prototype.

2) EXPERIMENTAL SETUP CONFIGURATION

As experimental validation, the fabricated stair PS prototype, previously introduced in Fig. 20, was tested in the frequency band from 2 GHz to 3 GHz. Similar to all classical microwave circuits, the stair PS SB-NGD test is based on the S-parameter analysis. The tests were realized with

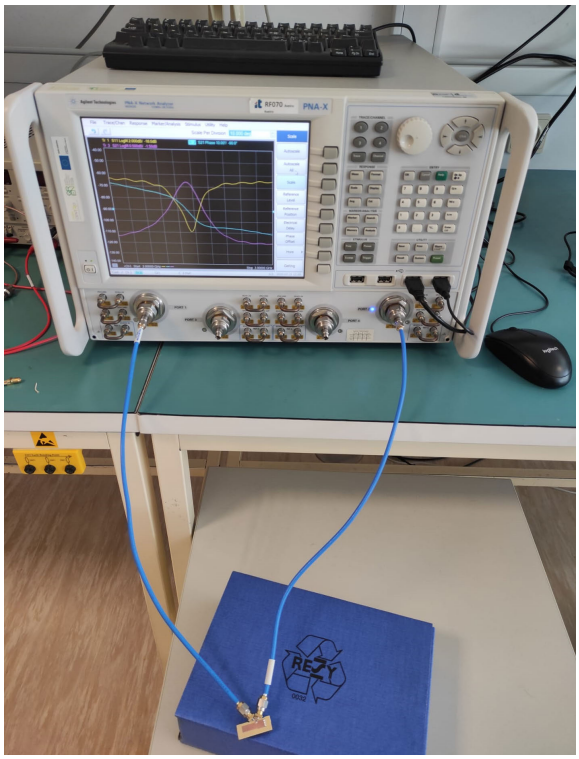

FIGURE 21. Configuration of the stair PS SB-NGD prototype experimental setup.

TABLE 7. Specifications of the tested two-step stair PS.

Parameters	Lumped		Distributed		Measurement	
	BW_L	BW_H	BW_L	BW_H	BW_L	BW_H
$f_{\min}$ (GHz)	2	2.6	2	2.6	2	2.6
$f_{\max}$ (GHz)	2.3	3.0	2.3	2.9	2.3	2.9
Φ_{mean} (°)	-66	-102	-67.4	-103	-70	-104
$\Delta\Phi$ (°)	+/-2.1	+/-3.2	+/-3	+/-2.4	+/-4	+/-2
$\Delta S_{21}(f_o)$ (dB)	0.82	1.35	1	1.28	0.88	0.94

10 MHz to 26.5 GHz PNA-X N5242A Network Analyzer from Keysight Technologies®. The experimental setup can be seen in Fig. 21.

During the measurement campaign, the test was made under SOLT calibration. The next paragraph will discuss between the simulated and measured results.

3) STAIR PS PROTOTYPE MEASUREMENT VALIDATION

Fig. 22 displays the comparisons between the (lumped and distributed) simulated and measured phase shift and GD results. As expected, they confirm undeniably the two-step stair PS functions. This PoC confirms the feasibility of stair PS. Table 7 summarizes the stair PS specifications.

A good correlation of stair phase values can be underlined with the measured one:

- In the first bandwidth, BW_L = 2-2.3 GHz, where we have a phase shift of $-70°\pm4°$.
- In the 2nd bandwidth, BW_H = 2.6-3.0 GHz, the step phase is shifted to $-104°\pm2°$.

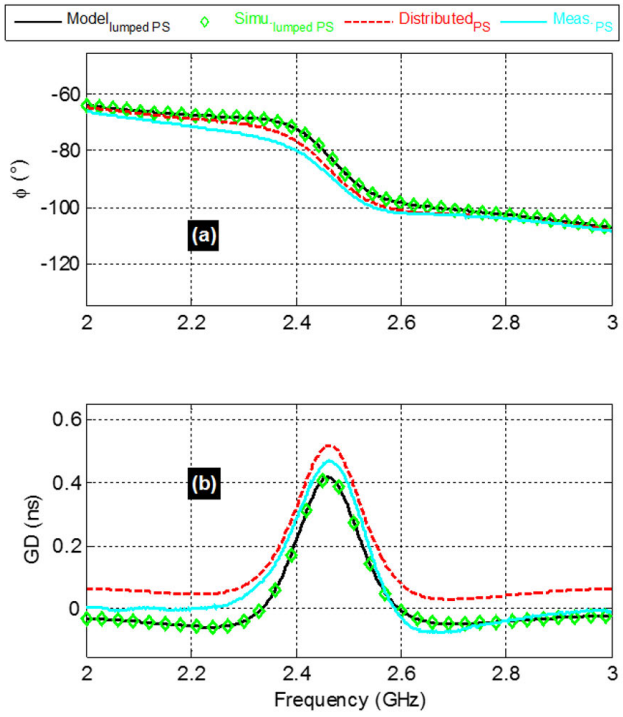

FIGURE 22. Simulated and measured, (a) transmission phase and (b) GD of the stair PS shown in Fig. 20.

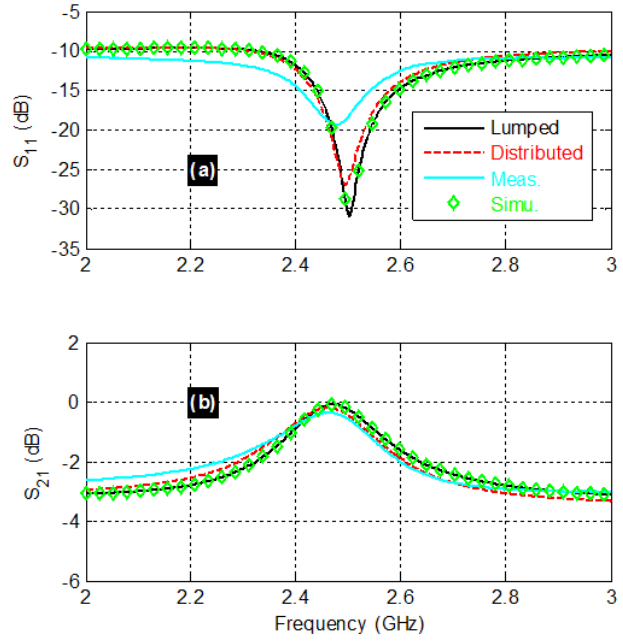

FIGURE 23. Simulated and measured (a) S_{11} and (b) S_{21} of the stair PS shown in Fig. 20.

Furthermore, the associated reflection and transmission coefficients of the stair PS PoC are plotted in Fig. 23. They show a good access matching between the two bands (BW_L and BW_H) and the PS flatness transmission coefficient less than 3 dB through the whole range (2-3 GHz).

VII. CONCLUSION

An original theory of SB-NGD circuit is presented. The proposed SB-NGD passive topology was inspired from the LP-NGD cell and the LP-to-SB circuit transform. The S-parameter model is established for the NGD analysis. The different properties of the SB-NGD function are developed.

To confirm the feasibility of the SB-NGD theory, a circuit PoC has been designed and simulated. Sensitivity analyses with respect to the constituting lumped component parameters are performed. It was reported how the SB-NGD response can be sensitivity to the three circuit parameters. An example of SB-NGD circuit application is developed to design a stair PS function with phase shift independent to the frequency. The principle of the stair PS is introduced. Simulations and experimentations illustrate the feasibility of the SB-NGD circuit-based stair PS in two frequency bandwidths.

The present research result is a pioneering work about the design of the future communication system. In this optic, the developed stair PS concept can be useful in the future for designing phase array system of innovative multi-beam antenna for the improvement of RF and microwave system control [41].

REFERENCES

[1] J. Zhang, S. Zhang, Z. Ying, A. S. Morris, and G. F. Pedersen, "Radiation-pattern reconfigurable phased array with p-i-n diodes controlled for 5G mobile terminals," *IEEE Trans. Microw. Theory Techn.*, vol. 68, no. 3, pp. 1103–1117, Mar. 2020.
[2] V. Kallnichev, "Analysis of beam-steering and directive characteristics of adaptive antenna arrays for mobile communications," *IEEE Antennas Propag. Mag.*, vol. 43, no. 3, pp. 145–152, Jun. 2001.
[3] S.-H. Yan and T.-H. Chu, "A beam-steering and-switching antenna array using a coupled phase-locked loop array," *IEEE Trans. Antennas Propag.*, vol. 57, no. 3, pp. 638–644, Mar. 2009.
[4] A. Hakkarainen, J. Werner, K. R. Dandekar, and M. Valkama, "Widely-linear beamforming and RF impairment suppression in massive antenna arrays," *J. Commun. Netw.*, vol. 15, no. 4, pp. 383–397, Aug. 2013.
[5] Y. Li, M. F. Iskander, Z. Zhang, and Z. Feng, "A new low cost leaky wave coplanar waveguide continuous transverse stub antenna array using metamaterial-based phase shifters for beam steering," *IEEE Trans. Antennas Propag.*, vol. 61, no. 7, pp. 2619–2625, Jul. 2013.
[6] S. S. Oh and L. Shafai, "Compensated circuit with characteristics of lossless double negative materials and its application to array antennas," *IET Microw., Antennas Propag.*, vol. 1, no. 1, pp. 29–38, Feb. 2007.
[7] M. A. Antoniades and G. V. Eleftheriades, "Compact linear lead/lag metamaterial phase shifters for broadband applications," *IEEE Antennas Wireless Propag. Lett.*, vol. 2, pp. 103–106, 2003.
[8] G. V. Eleftheriades, O. Siddiqui, and A. K. Iyer, "Transmission line for negative refractive index media and associated implementations without excess resonators," *IEEE Microw. Wireless Compon. Lett.*, vol. 13, no. 2, pp. 51–53, Feb. 2003.
[9] O. F. Siddiqui, M. Mojahedi, and G. V. Eleftheriades, "Periodically loaded transmission line with effective negative refractive index and negative group velocity," *IEEE Trans. Antennas Propag.*, vol. 51, no. 10, pp. 2619–2625, Oct. 2003.
[10] S. Lucyszyn and I. D. Robertson, "Analog reflection topology building blocks for adaptive microwave signal processing applications," *IEEE Trans. Microw. Theory Techn.*, vol. 43, no. 3, pp. 601–611, Mar. 1995.
[11] C. D. Broomfield and J. K. A. Everard, "Broadband negative group delay networks for compensation of oscillators, filters and communication systems," *Electron. Lett.*, vol. 36, no. 23, pp. 1931–1933, Nov. 2000.
[12] K.-P. Ahn, R. Ishikawa, and K. Honjo, "Group delay equalized UWB InGaP/GaAs HBT MMIC amplifier using negative group delay circuits," *IEEE Trans. Microw. Theory Techn.*, vol. 57, no. 9, pp. 2139–2147, Sep. 2009.

[13] B. Ravelo, S. Lalléchère, A. Thakur, A. Saini, and P. Thakur, "Theory and circuit modeling of baseband and modulated signal delay compensations with low- and band-pass NGD effects," *AEU Int. J. Electron. Commun.*, vol. 70, no. 9, pp. 1122–1127, Sep. 2016.
[14] T. Shao, Z. Wang, S. Fang, H. Liu, and Z. N. Chen, "A full-passband linear-phase band-pass filter equalized with negative group delay circuits," *IEEE Access*, vol. 8, pp. 43336–43343, 2020.
[15] W. Alomar and A. Mortazawi, "Method of generating negative group delay in phase arrays without using lossy circuits," in *Proc. IEEE Int. Wireless Symp. (IWS)*, Beijing, China, Apr. 2013, pp. 1–4.
[16] W. Alomar and A. Mortazawi, "Elimination of beam squint in uniformly excited serially fed antenna arrays using negative group delay circuits," in *Proc. IEEE Int. Symp. Antennas Propag.*, Chicago, IL, USA, Jul. 2012, pp. 1–2.
[17] H. Mirzaei and G. V. Eleftheriades, "Arbitrary-angle squint-free beamforming in series-fed antenna arrays using non-foster elements synthesized by negative-group-delay networks," *IEEE Trans. Antennas Propag.*, vol. 63, no. 5, pp. 1997–2010, May 2015.
[18] A. Mortazawi and W. Alomar, "Negative group delay circuit," U.S. Patent US20 160 093 958, Mar. 31, 2016.
[19] M. Zhu and C.-T.-M. Wu, "Reconfigurable series feed network for squint-free antenna beamforming using distributed amplifier-based negative group delay circuit," in *Proc. 49th Eur. Microw. Conf. (EuMC)*, Paris, France, Oct. 2019, pp. 256–259.
[20] H. Mirzaei and G. V. Eleftheriades, "Realizing non-Foster reactive elements using negative-group-delay networks," *IEEE Trans. Microw. Theory Techn.*, vol. 61, no. 12, pp. 4322–4332, Dec. 2013.
[21] T. Zhang, R. Xu, and C.-T. M. Wu, "Unconditionally stable non-foster element using active transversal-filter-based negative group delay circuit," *IEEE Microw. Wireless Compon. Lett.*, vol. 27, no. 10, pp. 921–923, Oct. 2017.
[22] B. Ravelo, M. Le Roy, and A. Perennec, "Application of negative group delay active circuits to the design of broadband and constant phase shifters," *Microw. Opt. Technol. Lett.*, vol. 50, no. 12, Dec. 2008, pp. 3077–3080.
[23] B. Ravelo, A. Pérennec, and M. L. Roy, "Synthesis of frequency-independent phase shifters using negative group delay active circuit," *Int. J. RF Microw. Comput.-Aided Eng.*, vol. 21, no. 1, pp. 17–24, Jan. 2011.
[24] B. Ravelo, "Distributed NGD active circuit for RF-microwave communication," *AEU Int. J. Electron. Commun.*, vol. 68, no. 4, pp. 282–290, Apr. 2014.
[25] L.-F. Qiu, L.-S. Wu, W.-Y. Yin, and J.-F. Mao, "Absorptive bandstop filter with prescribed negative group delay and bandwidth," *IEEE Microw. Wireless Compon. Lett.*, vol. 27, no. 7, pp. 639–641, Jul. 2017.
[26] Z. Wang, Y. Cao, T. Shao, S. Fang, and Y. Liu, "A negative group delay microwave circuit based on signal interference techniques," *IEEE Microw. Wireless Compon. Lett.*, vol. 28, no. 4, pp. 290–292, Apr. 2018.
[27] C.-T. M. Wu and T. Itoh, "Maximally flat negative group-delay circuit: A microwave transversal filter approach," *IEEE Trans. Microw. Theory Techn.*, vol. 62, no. 6, pp. 1330–1342, Jun. 2014.
[28] G. Liu and J. Xu, "Compact transmission-type negative group delay circuit with low attenuation," *Electron. Lett.*, vol. 53, no. 7, pp. 476–478, Mar. 2017.
[29] T. Shao, Z. Wang, S. Fang, H. Liu, and S. Fu, "A compact transmission line self-matched negative group delay microwave circuit," *IEEE Access*, vol. 5, pp. 22836–22843, 2017.
[30] H. Choi, Y. Jeong, J. Lim, S.-Y. Eom, and Y.-B. Jung, "A novel design for a dual-band negative group delay circuit," *IEEE Microw. Wireless Compon. Lett.*, vol. 21, no. 1, pp. 19–21, Jan. 2011.
[31] G. Chaudhary, Y. Jeong, and J. Lim, "Miniaturized dual-band negative group delay circuit using dual-plane defected structures," *IEEE Microw. Wireless Compon. Lett.*, vol. 24, no. 8, pp. 521–523, Aug. 2014.
[32] T. Shao, S. Fang, Z. Wang, and H. Liu, "A compact dual-band negative group delay microwave circuit," *Radioengineering*, vol. 27, no. 4, pp. 1070–1076, Dec. 2018.
[33] X. Zhou, B. Li, N. Li, B. Ravelo, X. Hu, Q. Ji, F. Wan, and G. Fontgalland, "Analytical design of dual-band negative group delay circuit with multi-coupled lines," *IEEE Access*, vol. 8, pp. 72749–72756, 2020.
[34] B. Ravelo, "Similitude between the NGD function and filter gain behaviours," *Int. J. Circuit Theory Appl.*, vol. 42, no. 10, pp. 1016–1032, Oct. 2014.
[35] B. Ravelo, "First-order low-pass negative group delay passive topology," *Electron. Lett.*, vol. 52, no. 2, pp. 124–126, Jan. 2016.
[36] B. Ravelo, "On the low-pass, high-pass, bandpass and stop-band NGD RF passive circuits," *URSI Radio Sci. Bull.*, vol. 2017, no. 363, pp. 10–27, Dec. 2017.
[37] M. Guerin, F. Wan, K. Gorshkov, X. Huang, B. Tishchuk, F. E. Sahoa, G. Chan, S. Baccar, W. Rahajandraibe, and B. Ravelo, "High-pass NGD characterization of resistive-inductive network based low-frequency circuit," *COMPEL Int. J. Comput. Math. Electr. Electron. Eng.*, vol. 40, no. 5, pp. 1032–1049, Oct. 2021.
[38] R. Yang, X. Zhou, S. S. Yazdani, E. Sambatra, F. Wan, S. Lalléchère, and B. Ravelo, "Analysis, design and experimentation of high-pass negative group delay lumped circuit," *Circuit World*, pp. 1–25, 2021, doi: 10.1108/CW-07-2020-0131.
[39] M. Guerin, Y. Liu, A. Douyere, G. Chan, F. Wan, S. Lallechere, W. Rahajandraibe, and B. Ravelo, "Design and synthesis of inductorless passive cell operating as stop-band negative group delay function," *IEEE Access*, vol. 9, pp. 100141–100153, 2021.
[40] S. Fenni, F. Haddad, K. Gorshkov, B. Tishchuk, A. Jaomiary, F. Marty, G. Chan, M. Guerin, W. Rahajandraibe, and B. Ravelo, "AC low-frequency characterization of stop-band negative group delay circuit," *Prog. Electromagn. Res. C*, vol. 115, pp. 261–276, 2021.
[41] H. Liu, S. Gao, and T. H. Loh, "Compact dual-band antenna with electronic beam-steering and beamforming capability," *IEEE Antennas Wireless Propag. Lett.*, vol. 10, pp. 1349–1352, 2011.

BLAISE RAVELO (Member, IEEE) is currently a University Full Professor with NUIST, Nanjing, China. His research interest includes multi-physics and electronics engineering. He is a Lecturer on circuit and system theory, STEM (science, technology, engineering and maths), and applied physics. He is a pioneer of the negative group delay (NGD) concept about $t < 0$ signal travelling physical space. This extraordinary concept is potentially useful for anticipating and prediction all kind of information. He was the Research Director of 11 Ph.D. students (ten defended), postdocs, research engineers, and master internships. With U.S., Chinese, Indian, European, and African partners, he is actively involved and contributes on several international research projects (ANR, FUI, FP7, INTERREG, H2020, Euripides^2, Eurostars). He is a member of *Electronics Letters* (IET) Editorial Board as a Circuit and System Subject Editor. He has been a member of the Scientific Technical Committee of Advanced Electromagnetic Symposium (AES), since 2013. He is ranked in Top 2% world's scientists based on years (2020–2021) by Stanford University, USA (https://elsevier.digitalcommonsdata.com/datasets/btchxktzyw/3). He has Google Scholar H-index (2021) = 24 and i10-index (2021) = 72. He is a member of the research groups IEEE, URSI, GDR Ondes, and Radio Society, and (co) authors of more than 360 scientific research papers in new technologies published in international conference and journals. He is an IEEE Member since 2007 and regularly invited to review papers submitted for publication to international journals (IEEE TRANSACTIONS ON MICROWAVE THEORY AND TECHNIQUES, IEEE TRANSACTIONS ON CIRCUITS AND SYSTEMS, IEEE TRANSACTIONS ON ELECTROMAGNETIC COMPATIBILITY, IEEE TRANSACTIONS ON INDUSTRIAL ELECTRONICS, IEEE ACCESS, IET CDS, and IET MAP) and books (Wiley and Intech Science).

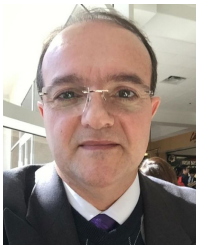

GLAUCO FONTGALLAND (Senior Member, IEEE) was born in Fortaleza, Ceará, Brazil, in March 1966. He was graduated and the M.S. degree in electrical engineering from the Universidade Federal de Campina Grande (UFCG), Campina Grande, Brazil, 1990 and 1993, respectively, and the Ph.D. degree in electronics from the Institut National Polytechnique de Toulouse—ENSEEIHT (1999), Toulouse, France, where his thesis work was nominated for the Leopold Escande Award 1999.

From 2010 to 2012, he was a Visiting Scholar at ElectroScience Laboratory, The Ohio State University (OSU), Columbus, OH, USA. He is currently a Full Professor with the Universidade Federal de Campina Grande (UFCG), Campina Grande, Brazil, where he develops research on: electromagnetic modeling, EMC, EMI, ESD, RFID, UWB, propagation, and antennas for various applications. He has published more than 200 papers in journal and conferences.

Prof. Fontgalland is a member of the Sociedade Brasileira de Micro-ondas e Optoeletrônica (SBMO), Sociedade Brasileira de Eletromagnetismo (SBMag), Sociedade Brasileira de Microeletrôncia (SBMicro), and The Applied Computational Electromagnetics Society (ACES). He is the past IEEE AP-S Chapter Chair and a member of the 2020 IEEE AP-S Student Design Contest and 2020 IEEE AP-S Field Awards Evaluation. Since 2019, he is an Associate Editor at IEEE Latin America Transactions.

HUGERLES S. SILVA (Member, IEEE) received the B.Sc., M.Sc., and Ph.D. degrees in electrical engineering from UFCG, Brazil, in 2014, 2016, and 2019, respectively. He is currently a Postdoctoral Student at the Telecommunications Institute, University of Aveiro, Portugal. His main research interests include wireless communication, digital signal processing, and wireless channel modeling.

JAMEL NEBHEN (Member, IEEE) received the M.Sc. degree in microelectronics from the National Engineering School of Sfax, Tunisia, in 2007, and the Ph.D. degree in microelectronics from Aix-Marseille University, France, in 2012. From 2012 to 2018, he worked as a Postdoctoral Researcher at the LIRMM-Lab Montpellier, IM2NP-Lab Marseille, ISEP Paris, LE2I-Lab Dijon, Lab-Sticc Telecom Bretagne Brest, and IEMN-Lab Lille, France. Since 2019, he joined the Prince Sattam Bin Abdulaziz University, Al-Kharj, Saudi Arabia, as an Assistant Professor. His research interests include the design of analog and RF integrated circuits, the IoT, biomedical circuit, and sensors instrumentation.

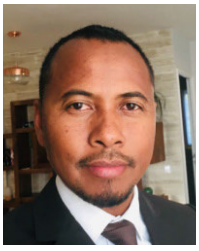

WENCESLAS RAHAJANDRAIBE (Member, IEEE) received the B.Sc. degree in electrical engineering from the University of Nice Sophia Antipolis, France, in 1996, the M.Sc. degree (Hons.) in electrical engineering from the Science Department, University of Montpellier, France, in 1998, and the Ph.D. degree in microelectronics from the University of Montpellier. In 1998, he joined the Montpellier Laboratory of Computer Science, Robotics, and Microelectronics (LIRMM), Microelectronics Department, University of Montpellier. In 2003, he joined the Microelectronic Department, Institute Materials Microelectronics Nanosciences of Provence (IM2NP), Marseille, France, where he was an Associate Professor. Since 2014, he has been a Professor at Aix-Marseille University, where he heads the Integrated Circuit Design Group of the IM2NP Laboratory. He is currently a Full Professor with Aix-Marseille University. He is regularly involved to participate and to lead national and international research projects (ANR, H2020, FP7 KIC-InnoEnergy). He directed and co-supervised 18 Ph.D. and 15 master students. His research interests involve AMS and RF circuit design from transistor to architectural level. His present research activity is focused on ultralow power circuit design for smart sensor interface and embedded electronic in bioelectronic and e-health applications, wireless systems, design technique, and architecture for multi-standard transceiver. He is the author or coauthor of more than 150 papers published in refereed journals and conferences and holds 11 patents. He is an Expert of the ANR, the French Agency for Research. He has served on program committees of IEEE NEWCAS and ICECS. He has been and is a Reviewer of contributions submitted to several IEEE conferences and journals, such as ISCAS, NEWCAS, MWSCAS, ESSCIRC, ESSDERC, RFIC, IEEE Transactions on Circuits and Systems—I, IEEE Transactions on Circuits and Systems—II, and *Electronics Letters* (IET).

MATHIEU GUERIN (Member, IEEE) received the Engineering degree in microelectronics and telecommunications from Polytech Marseille, in 2010, and the master's degree (by Research) in integrated circuits design and the Ph.D. degree from Aix-Marseille University, in December 10, 2013. He worked as the Technical Leader of the Analog and Radio-Frequency Design Team at IDEMIA-StarChip for five years and designed chips embedded in SIM cards and contactless bank cards with biometric recognition. In 2020, he joined Aix-Marseille University, as an Assistant Professor, where he joined the CCSI Team of the IM2NP Laboratory. His research interest includes the design and synthesis of circuits in digital electronics. He is also working on methods of modeling and characterizing circuits in analog electronics.

GEORGE CHAN (Senior Member, IEEE) received the B.Eng. (Hons.) degree in electronic and communication engineering from the City University of Hong Kong and the M.Sc. degree in electronic and information engineering from The Hong Kong Polytechnic University.

He is currently a Senior Product Safety Engineer at ASM Pacific Technology Ltd. His research interests include electromagnetic safety, EMC measurement, and EMC management. He has coauthored several technical publications in international journals and conference proceedings. He is a member of IEEE EMC Society TC1 on EMC Management. He is also a member of the IEEE International Committee for Electromagnetic safety (ICES) Standards Coordinating Committee (SCC39) and a TC95 Sub-Committee Member. He is an International Electrotechnical Commission (IEC) Expert and a Committee Member of IEC TC106/PT63184 on Method for the assessment of electric, magnetic and electromagnetic fields associated with human exposure.

FAYU WAN (Member, IEEE) received the Ph.D. degree in electronic engineering from the University of Rouen, Rouen, France, in 2011. From 2011 to 2013, he was a Postdoctoral Fellow with the Electromagnetic Compatibility Laboratory, Missouri University of Science and Technology, Rolla. He is currently a Full Professor with the Nanjing University of Information Science & Technology, Nanjing, China. His current research interests include negative group delay circuits, electrostatic discharge, electromagnetic compatibility, and advanced RF measurement.